EXPERIMENT NO. 3

INVESTIGATION OF FLOW PAST A CIRCULAR CYLINDER

Submitted by:

Kush Jani

AEROSPACE AND OCEAN ENGINEERING DEPARTMENT

VIRGINIA POLYTECHNIC INSTITUTE AND STATE UNIVERSITY

BLACKSBURG, VIRGINIA

20 MARCH 2025

EXPERIMENT PERFORMED 20 FEBUARY 2025

LAB TEACHING ASSISTANT: HEEJIN KIM

INVESTIGATION OF FLOW PAST A CIRCULAR CYLINDER

Kush Jani[1]
Virginia Tech, Blacksburg, VA 24060

I. Introduction

Understanding the pressure distributions, and thus the lift and drag forces, about bodies accurately is a critical problem and forms the basis of fluid dynamics as a field and the aerospace industry as a whole. However, the problem of properly identifying the pressure distribution is non-trivial, and the complexities of doing such necessitated the use of simplifications up until the recent advance of computational power. Nonetheless, the theoretical models with simplifications created to solve for the pressure distributions about objects remain in use even with modern computing power for some applications and thus need validation or analysis to highlight shortcomings in the models. Inviscid theory is one such theoretical model in which the viscous effects of fluids created by internal friction is assumed negligible and thus ignored. However, this theory becomes increasingly inaccurate near boundary layers caused by disturbances in flows and one of the classic examples of the inaccuracy of the model is the flow around a circular cylinder. For this scenario, the inviscid theory predicts zero drag and assumes the flow remains attached to its surface whereas real world examples demand the presence of drag and wakes caused by viscous boundary layer effects and flow separation. In this investigation, the flow past a circular cylinder is analyzed in the real world to highlight the discrepancies between the inviscid theoretical predictions and the true measured values of pressure distributions. For the investigation, the objectives were:

1. At a fixed Reynolds, compare the experimental pressure distribution and drag to the inviscid theory for the irrotational non-lifting cylinder.
2. Vary Reynolds number to determine its effect on the pressure distribution coefficient and compare with the pressure distribution from inviscid theory for the irrotational non-lifting cylinder.
3. Vary the Reynolds number to determine its effect on the wake and compare with the wake predicted from inviscid theory.
4. Identify the point where C_{po} falls to 0.98 to determine the wake edge

While objectives 3 and 4 were limited in being met due to time constraints faced as a result of extensive experimental setup and calculations, objectives 1 and 2 were met and measurements were made in laboratory conditions on a circular cylinder as shown in Fig. 1. As shown in Fig. 1, the test cylinder was oriented such that the flow would be perpendicular to the length of the cylinder (where length is defined as shown in Fig. 2). Further shown in Fig. 1 are the various pressure sensing equipment utilized to measure and plot the pressure distribution about the cylinder. There are 36 different pressure sensing ports, allowing a pressure measurement to be made for every 10 degrees around the cylinder.

As described in brief prior, the goals of the experiment involve analyzing the experimentally measured values for the pressure distribution about a circular cylinder for comparison with the inviscid theory predictions for pressure distribution. According to inviscid theory, the pressure coefficient distribution about a circular cylinder is predicted to be given by the equation

$$C_p = 1 - 4sin^2\theta \tag{1}$$

where θ is the angle measured from the back of the cylinder as shown in Fig. 3. This equation is derived from the equation for the coefficient of pressure

$$C_p = {p - p_\infty}\Big/{\frac{1}{2}\rho U_\infty^2} \tag{2}$$

and from Bernoulli's equation

$$p + \frac{1}{2}\rho u^2 = p_\infty + \frac{1}{2}\rho U^2 \tag{3}$$

which are manipulated algebraically to find the aforementioned Eq. 1. By plotting Eq. 1 for 10-degree increments of θ and comparing said plot with the measured values by the 36 sensors that also provide 10-degree increments for pressure coefficients, a comparison can be made between the theoretical and measured values.

[1] Undergraduate student, Aerospace & Ocean Engineering Department.

The theoretical and measured values can be further compared with the measured and theoretical predictions found by Bertin and Smith, shown in Fig. 4. Furthermore, the coefficient of pressure measured along the cylinder can be identified and compared with expected values due to viscous effects, implying the presence of a wake edge.

Further background useful for the report is the nature of digital pressure scanners such as the Esterline 9816/98RK pressure scanner used for this experiment. This scanner uses piezoresistive pressure sensors which operate differently than pitot tubes or manometers and allows for the pressure to be converted to an electronic signal that is processed to provide the pressure readings.

The remainder of this report is organized as follows: Section II describes the experimental setup, apparatuses, and techniques used to conduct the experiment while going into more detail on the specific numerical methods used to plot the theoretical pressure distribution and corresponding MATLAB code. Section III describes the results obtained from the experiment, compares the results obtained against inviscid theory, and overviews shortcomings in the experiment/meeting objectives for advances in further experimentation. Finally, Section IV describes the implications and conclusions gleaned from the experimental results while also overviewing the insights gained in procedures and techniques employed throughout the experiment and what further work could be done in subsequent investigations to fully meet the unmet/partially met objectives.

II. Apparatus and Techniques

A. Open Jet Wind Tunnel

The experiment was conducted in the Virginia Tech 0.7m Subsonic Open-Jet Wind Tunnel, which is designed to produce a uniform stream of air for aerodynamic testing. The wind tunnel itself is a blower type open circuit facility residing on a steel base and made up of aluminum composite panels and aluminum frame. The fan providing the wind for the tunnel is a 30hp BC-SW Size 365 Twin City centrifugal fan which discharges into a 6° diffuser that is 4 meters long. The flow then settles in a 1.47m by 1.78m settling chamber where 0.01m-cell size, 0.09m long honeycomb and three turbulence reduction screens made of 0.3mm-diameter fiberglass screen with a 55% open area ratio that allow for the flow to become uniform and non-turbulent. The end of the tunnel has a 5.5:1 contraction nozzle. The maximum operational fan speed is 1180 RPM, corresponding to a maximum freestream velocity in the test section of approximately 30 m/s. The freestream velocity was monitored throughout the experiment using a reference Pitot-static probe (further discussed in Section D). Fig. 5 depicts, from right to left, the air intake for the fan, the fan housing, diffuser, settling chamber, control center, open test section, and jet catcher. The jet catcher, located 1.2 meters past the nozzle exit, is used to deflect and defuse the stream of air from the wind tunnel and uses two fiberglass high-loss screens inside the jet catcher along with further high-loss screens at the bottom and top of the jet catcher to minimize flow velocity before entering the room. The wind tunnel is controlled via the Open-Jet Wind Tunnel Operation Control MATLAB code, which allows for GUI based access to the fan RPM, scanner calibration, traverse control for the Pitot-static probe, and atmospheric conditions in the room.

B. Circular Cylinder Test Section

The cylindrical model tested in the open test section was a smooth, circular cylinder model constructed from Plexiglas, with a diameter of 140 mm and a length of 462 mm. The model was capped on both ends by circular plates with diameters of 305 mm, allowing the flow effects caused by the edges of the cylinder to be minimized in order to better approximate two-dimensional flow around the center of the model. The cylinder was mounted 25 cm downstream of the nozzle exit. While the model is mounted such that it is able to rotate about its axis, this ability was not used for the experiment performed. The cylinder has 36 one-millimeter diameter pressure taps at 10 degree intervals along the perimeter of the cylinder at the midlength. These taps transmit the pressure through 3 mm outside diameter Tygon tubes.

C. Pressure Distribution Sensor System

In order to measure the pressure distribution about the circular cylinder model, an Esterline 9816/98RK pressure scanner was used. This scanner has 48 channels with a range of +/-10 inches of water column and a rated accuracy of +/-0.05% full scale. The pressure scanner for this investigation was setup such that ports/taps 1 through 36 on the cylinder are connected to channels 1 through 36 on the Esterline pressure scanner. Channels 42 and 43 of the Esterline pressure scanner are reserved for the traversing probe's static and stagnation pressures respectively. Channel 47 is similarly reserved for the settling chamber's static pressure. The scanner uses ethernet to connect to the computer via an RJ-45 cable. As described in Section A, a MATLAB GUI controls the scanner and allows for real-time visualization of the pressure distribution

along with the ability to store collected data. The code outputs the pressure as measured by the scanner directly, which is thus in inches of water. This thus requires conversion using the equation

$$p = \rho_{water} g h \tag{4}$$

in order to calculate the pressure relative to atmospheric pressure. Finally, the pressure sensor is set up in such a fashion for this investigation as to have the first tap, corresponding to channel 1, be for the foremost part of the cylinder and thus correspond to 180 degrees on the output data.

D. Pitot Probe and Other Equipment

The Pitot-static probe used in this investigation is a Dwyer model 160 Pitot-static probe as shown in Fig 6. This probe was mounted on three-axis computer-controlled traverse gear which itself is a custom Velmex VMS linear slide system. The traverse gear has a programmable traverse resolution of 0.25 mm and setup for this investigation such that +x points downstream, +y points along the length of the test cylinder away from the computer control center/operators, and +z points to the floor. This traversal capability would allow for the manipulation of the Pitot-static probe such that various locations could be measured in order to find a location with a C_{po} of 0.98 and thus the wake edge. The default location used throughout this investigation was 140 mm downstream of the midlength of the circular cylinder. A Raspberry Pi computer was used for data acquisition, controlling the pressure scanner, and recording temperature and atmospheric pressure. The accuracy of the SenseHat sensor on the Raspberry Pi for atmospheric pressure was ±0.1 millibar. A DS18B20 Digital Thermometer was attached to the side of the frame upstream of the open test section and measured air temperature with an accuracy of ±0.5 degrees Celsius. These instruments allowed for the calculation of the Reynolds number.

III. Results and Discussion

This section is formatted such that Method 1 describes the procedure and methodology used to meet the first objective, Method 2 describes the procedure used for the second objective, and Method 3 describes the procedure intended to be used for objectives three and four along with the limited results for objectives three and four obtained in this investigation.

A. Method 1: Comparison of Experimental Pressure Distribution with Theoretical for Fixed Reynolds Number

In order to determine the pressure distribution about the circular cylinder test section and meet the first objective for this investigation, the use of a fixed Reynolds number was necessary. Reynolds number for a flow is given by the equation

$$Re_D = \frac{U_\infty D}{\nu} \tag{5}$$

where U is the velocity of the freestream, D is the diameter of the circular test section, and ν is the kinematic viscosity. Since kinematic viscosity is not measurable by the instrumentation for this investigation is capable of measuring, a relation with other factors is needed to solve for kinematic viscosity. Kinematic viscosity is further defined by the dynamic viscosity and density as shown by the equation

$$\nu = \frac{\mu}{\rho} \tag{5}$$

where μ is the dynamic viscosity and ρ is the density of air. Since dynamic viscosity and density are also not directly measurable by the instrumentation for this investigation, further relations are needed to solve for dynamic viscosity. Dynamic viscosity is defined by Sutherland's equation

$$\mu = \frac{1.4578\times10^{-6} T^{1.5}}{T+110.4} \tag{6}$$

where T is the temperature in Kelvin. Density is defined by the ideal gas law equation

$$\rho = {}^{p}/_{RT} \tag{7}$$

where p is atmospheric pressure, R is the gas constant, and T is temperature. Since pressure and temperature are measurable via the instrumentation for this investigation, the Reynolds number can thus be calculated. For the first method, the wind tunnel fan was set to 100 RPM and relevant values for calculation of the Reynolds number were measured as shown in Table 1.

Table 1. Measured factors for Reynolds number calculations at 100 RPM.

RPM (rpm)	*Diameter* (m)	*T* (K)	p_{atm} (mbar)	U_∞ (m/s)

100	0.14	294.837	94649.12	2.084728

From these measured values, the density and dynamic viscosity can be calculated and thus the kinematic viscosity and Reynolds number for the RPM set to 100 can be found as shown below in Table 2.

Table 2. Derived factors for Reynolds number calculations at 100 RPM.

RPM (rpm)	*Density* (kg/m^3)	*μ* (Pa·s)	*ν* (m^2/s)	Re_D (N/A)
100	1.118543041	1.82122E-05	1.62821E-05	17925.3773

With the Reynolds number calculated as being subcritical due to having a value of 17925.3773, the next step in the investigation involved the acquisition of pressure distribution about the circular cylinder test section, conversion from native pressure sensor measurements in inches of water to pascals and calculation using the equation for pressure coefficient given as

$$C_p = {p - p_\infty}/{\frac{1}{2}\rho U_\infty^2} \tag{8}$$

The acquisition of pressure distribution involved using the aforementioned Open-Jet Wind Tunnel Operation Control MATLAB code, and data for pressure values for ports 1 through 36 were given as shown in Table 3.

Table 3. Measured pressures for C_p calculations at 100 RPM.

20-Feb-2025 17:38:27 Data for RPM 100

1	0.01001	***9***	-0.00152	***17***	-0.00234	***25***	-0.00194	***33***	0.003583	***41***	0.000897
2	0.00847	***10***	-0.00168	***18***	-0.00202	***26***	-0.00211	***34***	0.006386	***42***	-0.00032
3	0.00584	***11***	-0.00171	***19***	-0.00244	***27***	-0.00179	***35***	0.008595	***43***	-0.00222
4	0.0032	***12***	-0.00212	***20***	-0.00249	***28***	-0.00189	***36***	0.009808	***44***	-0.00036
5	-0.00015	***13***	-0.00199	***21***	-0.00251	***29***	-0.00376	***37***	-0.00011	***45***	0.001216
6	-0.00214	***14***	-0.00203	***22***	-0.00233	***30***	-0.00395	***38***	-0.00077	***46***	0.000641
7	-0.00306	***15***	-0.0021	***23***	-0.00217	***31***	-0.00295	***39***	0.002364	***47***	0.009496
8	-0.00285	***16***	-0.00213	***24***	-0.0022	***32***	6E-06	***40***	0.001845	***48***	0.000609

Uref (m/s)	***Amb Temperature***	***Amb Pressure***
2.084728	21.687000	946.491200

During the investigation, the data was stored under Obj1.txt after formatting and subsequently converted from pressure units of inches of water to Pascals before being inserted into Eq. 8 to calculate and plot the C_p via MATLAB code as shown in Fig. 7. The resulting graph from running the code in Fig. 7 is shown in Fig. 8. Notably, the MATLAB code calculates a "diffp" variable that was ultimately not used and provided a temporary source of error as the output pressure values from the Open-Jet Wind Tunnel Operation Control MATLAB code automatically calculates for the difference in atmospheric versus measured pressured about the cylinder, allowing the C_p equation to simply require the acquired data values in the numerator.

In order to compare these measured results against inviscid theory, the calculation of C_p about a circular cylinder using inviscid theory necessarily must be performed and plotted for increments of 10 degrees. As discussed in the introduction, the equation for the pressure coefficient about a circular cylinder can be derived from Bernoulli's equation as well as the equation for coefficient of pressure, which results in

$$C_p = 1 - 4sin^2\theta \tag{1}$$

where θ is the angle measured from the back of the cylinder as shown in Fig 3. Utilizing this equation, MATLAB code (shown in Fig. 9) can plot the C_p about a circular cylinder predicted by inviscid results and by doing so, Fig. 10 is generated. Further discussion is done in Section IV, but notably the results from this investigation and method accurately match those of *From Boundary Layer Theory* by H. Schlichting (1968), (as shown in Fig. 4 from Bertin and Smith).

B. Method 2: Comparison of Experimental Pressure Distribution with Theoretical for Varied Reynolds Numbers

One of the notable results from the derivations of Reynolds number shown in Method 1 is that the Reynolds number only depends on the generally negligibly changing factors of atmospheric pressure and temperature alongside the variable freestream velocity factor. As a result, by changing the freestream velocity and only the freestream velocity, the Reynolds number can directly be changed.

In order to meet the second objective set forth for this investigation, the freestream velocity, and thus

Reynolds number, necessarily must be changed and was done so via the modulation of the RPM. The RPM values tested went from 100 to 500 with increments of 100 per trial. These RPM values were chosen rather than evenly spacing out RPM values from minimum to maximum in order to prevent the extended use of the wind tunnel at high RPMs due to the significant noise produced at high RPMs. The measured values for RPMs from 100 to 500 relevant for calculations of the Reynolds number are shown below in Table 4.

Table 4. Measured factors for Reynolds number calculations at 100 RPM.

RPM (rpm)	*Diameter* (m)	*T* (K)	p_{atm} (mbar)	U_∞ (m/s)
100	0.14	294.837	94649.12	2.084728
200	0.14	294.025	94738.45	4.611
300	0.14	294.9	94757.42	7.0103
400	0.14	295.025	94756.15	9.2839
500	0.14	295.15	94743.77	11.6488

From these measured values, the density and dynamic viscosity can be calculated and thus the kinematic viscosity and Reynolds number for the RPMs from 100 to 500 can be found as shown below in Table 5.

Table 5. Derived factors for Reynolds number calculations at 100 RPM.

RPM (rpm)	*Density* (kg/m^3)	μ (Pa·s)	ν (m^2/s)	Re_D (N/A)
100	1.118543041	1.82122E-05	1.62821E-05	17925.3773
200	1.122690686	1.81734E-05	1.61874E-05	39879.24594
300	1.119583677	1.82152E-05	1.62696E-05	60323.66181
400	1.119094319	1.82211E-05	1.6282E-05	79826.94913
500	1.118474218	1.82271E-05	1.62964E-05	100073.1294

With the Reynolds number calculated for all RPMs as being, the next step in the investigation followed the same procedure in Method 1 of acquiring the pressure distribution about the circular cylinder test section, conversion from native pressure sensor measurements in inches of water to pascals, and calculation using the equation for pressure coefficient.

The acquisition of pressure distribution once more used the Open-Jet Wind Tunnel Operation Control MATLAB code, and data for pressure values for ports 1 through 36 for RPMs of 200, 300, 400, and 500 are given below in Table 6, 7, 8, and 9 respectively.

Table 6. Measured pressures for Cp calculations at 200 RPM.

20-Feb-2025 18:52:34 Data for RPM 200

1	0.047	**9**	-0.01265	**17**	-0.01371	**25**	-0.01123	**33**	0.015066	**41**	0.001369
2	0.03947	**10**	-0.01222	**18**	-0.01291	**26**	-0.01332	**34**	0.029895	**42**	-0.00418
3	0.02752	**11**	-0.01289	**19**	-0.01289	**27**	-0.01153	**35**	0.041059	**43**	-0.01035
4	0.01217	**12**	-0.01359	**20**	-0.01294	**28**	-0.01202	**36**	0.046698	**44**	-0.00005
5	-0.0032	**13**	-0.01313	**21**	-0.01297	**29**	-0.01579	**37**	-0.00044	**45**	0.000816
6	-0.01475	**14**	-0.01386	**22**	-0.01342	**30**	-0.01945	**38**	-0.00056	**46**	0.000677
7	-0.01975	**15**	-0.01327	**23**	-0.01283	**31**	-0.01392	**39**	0.002416	**47**	0.046403
8	-0.01488	**16**	-0.01351	**24**	-0.01295	**32**	-0.00007	**40**	0.001763	**48**	0.000204

Uref (m/s)	***Amb Temperature***	***Amb Pressure***
4.611047	20.875000	947.384500

Table 7. Measured pressures for Cp calculations at 300 RPM.

20-Feb-2025 18:55:25 Data for RPM 300

1	0.10591	**9**	-0.0308	**17**	-0.03122	**25**	-0.03017	**33**	0.033538	**41**	0.001294
2	0.09028	**10**	-0.0306	**18**	-0.03071	**26**	-0.03103	**34**	0.068468	**42**	-0.00488
3	0.062	**11**	-0.03164	**19**	-0.03144	**27**	-0.02908	**35**	0.093787	**43**	-0.02302
4	0.02657	**12**	-0.03252	**20**	-0.03163	**28**	-0.02922	**36**	0.106494	**44**	-0.00014
5	-0.00861	**13**	-0.0322	**21**	-0.03156	**29**	-0.03512	**37**	-0.00045	**45**	0.001001

6	-0.03532	**14**	-0.03263	**22**	-0.03197	**30**	-0.04617	**38**	-0.0002	**46**	0.00099
7	-0.04758	**15**	-0.03219	**23**	-0.03216	**31**	-0.03373	**39**	0.002334	**47**	0.106972
8	-0.0344	**16**	-0.03258	**24**	-0.03213	**32**	-0.00247	**40**	0.001888	**48**	0.00011

Uref (m/s)	*Amb Temperature*	*Amb Pressure*
7.010319	21.750000	947.574200

Table 8. Measured pressures for Cp calculations at 400 RPM.

20-Feb-2025 18:57:16 Data for RPM 400

1	0.18732	**9**	-0.05429	**17**	-0.05782	**25**	-0.05583	**33**	0.059241	**41**	0.001218
2	0.15931	**10**	-0.05425	**18**	-0.05742	**26**	-0.05626	**34**	0.121275	**42**	-0.02222
3	0.10906	**11**	-0.0561	**19**	-0.058	**27**	-0.05377	**35**	0.166571	**43**	-0.04706
4	0.04652	**12**	-0.05745	**20**	-0.05849	**28**	-0.05383	**36**	0.189316	**44**	-0.00036
5	-0.01647	**13**	-0.05768	**21**	-0.05835	**29**	-0.06206	**37**	-0.00077	**45**	0.000813
6	-0.06343	**14**	-0.0588	**22**	-0.05758	**30**	-0.08153	**38**	-0.00085	**46**	0.000803
7	-0.08181	**15**	-0.05895	**23**	-0.05721	**31**	-0.05914	**39**	0.001562	**47**	0.187422
8	-0.05801	**16**	-0.05918	**24**	-0.05765	**32**	-0.00411	**40**	0.001039	**48**	0.000216

Uref (m/s)	*Amb Temperature*	*Amb Pressure*
9.283959	21.875000	947.561500

Table 9. Measured pressures for Cp calculations at 500 RPM.

20-Feb-2025 18:58:56 Data for RPM 500

1	0.29393	**9**	-0.08579	**17**	-0.09216	**25**	-0.0886	**33**	0.092937	**41**	0.001501
2	0.25044	**10**	-0.08653	**18**	-0.09138	**26**	-0.08857	**34**	0.191605	**42**	-0.01543
3	0.17107	**11**	-0.08874	**19**	-0.09261	**27**	-0.0854	**35**	0.263122	**43**	-0.06319
4	0.07267	**12**	-0.09101	**20**	-0.09342	**28**	-0.08478	**36**	0.299205	**44**	0.000156
5	-0.0265	**13**	-0.09082	**21**	-0.0931	**29**	-0.0945	**37**	-0.00049	**45**	0.000832
6	-0.09938	**14**	-0.09154	**22**	-0.09279	**30**	-0.12807	**38**	-0.00068	**46**	0.000998
7	-0.1279	**15**	-0.09156	**23**	-0.09148	**31**	-0.09269	**39**	0.002177	**47**	0.295057
8	-0.09073	**16**	-0.09233	**24**	-0.09145	**32**	-0.00732	**40**	0.001593	**48**	0.000691

Uref (m/s)	*Amb Temperature*	*Amb Pressure*
11.648854	22.000000	947.437700

These data values were stored in Obj2.txt to Obj5.txt for the respective RPMs used. The resulting graph from running the code shown in Fig. 11 is depicted in Fig. 12. In order to compare the results from the measured coefficient of pressure distributions about a circular cylinder as shown in Fig. 12 against the theoretical coefficient of pressure distributions about a circular cylinder, Fig. 10 can be reused since, as shown in Eq. 1 and the code for Fig. 10 from Fig. 9, the inviscid theory does not have the pressure distribution affected by the velocity of the flow or the Reynolds number. As a result, Fig. 10 is still applicable for use in comparison of inviscid theory predictions as the predictions are independent of Reynolds number, highlighting another shortcoming of the theory.

Further discussion of the conclusions and implications is done in Section IV. However, the graph generally shows an anomaly in the C_p measured about the cylinder. This discrepancy is likely due to the difference in time and thus ambient temperatures and pressures between the RPM 100 trial and all other trials since trials for RPMs of 200 to 500 were performed in rapid succession. Overall, the graph does generally show a trend of decreasing C_p distributions overall as the Reynolds number increases with the 500 RPM trial being of lowest C_p values overall. Also of note is the continued discrepancy between inviscid theory and experimental measurements regardless of the variance in Reynolds number.

C. Method 3: Comparison of Wake for Varied Reynolds Numbers

Due to time constraints on accessing the wind tunnel, meeting objectives three and four was not feasible. In order to perform objective three, the procedure planned for prior to experimentation involved measuring the pressure values using the Pitot-static probe for specific locations downstream of the cylinder in the open test section utilizing the traverse mechanism of the probe under a particular Reynolds number and

subsequently remeasuring the pressure values at the same locations for a different Reynolds number. This would allow a plot to be made of pressures measured by the Pitot probe and visualize the flow downstream of the cylinder, which would theoretically allow estimations or even definite identifications of the wake and wake edge to be made. These would subsequently be compared to the wake predicted by inviscid theory about a circular cylinder, which would predict the absence of a wake. In order to prove the presence of no wake predicted by inviscid theory, a modification was made to "Linear vortex panel method for airfoils" by William Devenport, as shown in Fig. 13, to plot a circle rather than an airfoil in order to represent a 2D slice of the cylinder undergoing 2D flow. The result of three streamlines placed above, on, and under the centerline of the circle is shown in Fig. 14 and demonstrates the prediction made by inviscid theory on the smooth reconvergence of flow, preventing the creation of a wake. In general, the inviscid theory can still be invalidated for the absence of a wake as smooth reconvergence of flow like that predicted by the theory would create a coefficient of pressure distribution that would be symmetric about the 0-degree line as seen in Fig. 10, which is not the correct distribution as seen in Fig. 8.

Furthermore, in order to meet objective four, the probe would be utilized again at various locations seemingly around the wake edge as predicted by the results of objective three. The stagnation pressure would be subsequently measured for these locations until the C_{po} value calculated using the equation

$$C_{po} = {p_o - p_\infty}/{p_{o\infty} - p_\infty} \tag{9}$$

Since the stagnation flow remains constant in the inviscid steady flow, the C_{po} would always be 1 and thus a way to define the wake edge is the location at which C_{po} falls to 0.98. By traversing across potential locations for the wake edge, the Pitot-static probe would be able to find locations whereby the subsequent calculations for C_{po} do indeed fall to 0.98 and thus prove the creation of a wake edge and wake to further invalidate the accuracy of inviscid theory for flow about a circular cylinder.

IV. Conclusion

The investigation conducted utilized various techniques to highlight shortcomings of inviscid theory predictions against experimental measurements for the real world. Measurements made by the instrumentations allowed for the recording of ambient pressures, temperatures, and freestream velocity which were subsequently used to tabulate the Reynolds number. Further measurements by the pressure sensor recorded the pressure distribution about the circular cylinder, allowing for the tabulation of the coefficient of pressure about the circular cylinder test section. The investigation used four different procedures, with the first procedure involving the calculation of the coefficient of pressure about the cylinder for a fixed Reynolds number before varying the Reynolds number to recalculate the coefficient of pressures and wake for the cylinder for procedures two and three respectively. Lastly, the fourth procedure involved analyzing the wake downstream of the cylinder from procedure three to approximate and subsequently identify the location of the wake edge for the location where C_{po} falls to 0.98. The following conclusions were made from the investigation:

1. The inviscid theory has significant shortcomings in predicting the coefficient of pressure distribution about a circular cylinder for subcritical Reynolds number airflow.
2. The inviscid theory has significant shortcomings in predicting the overall decrease in coefficient of pressure distribution about a circular cylinder for increasing but subcritical Reynolds number airflow.
3. The inviscid theory predicts the formation of no wake for flow about a circular cylinder and incorrect as this would imply a coefficient of pressure distribution such as the ones found in prior objectives/conclusions, which is not what is experimentally measured.

From the results gathered, comments can be made on the methodology and techniques used throughout the experiments. Firstly, the methodology for Method 1 was seemingly of great accuracy as the resulting plot as shown in Fig. 8 matched the measured values of Bertin and Smith to a large degree. However, some improvement could be made in the methodology for Method 2 by remeasuring the pressures for RPM 100 at a time closer to the times RPMs 200-500 were measured in order to minimize the differences in the ambient environment and thus the calculations for coefficient of pressure. Method 3 was greatly limited by time as measurements of pressure using the Pitot-static probe were not able to be made in the time available for the investigation and thus there was no pressure distribution plot that could have aided in Method 4 for approximating the location of the wake edge. However, Method 3 was still successful in invalidating inviscid theory as the conclusions made about the absence of a wake necessitating a symmetric coefficient of pressure distribution unlike the one measured fundamentally relied on the wake shortcomings of the theory and form

equally strong arguments against the theory for accurate prediction of flow about a circular cylinder.

The analysis for coefficient of pressure calculations for RPMs of 100 to 500 were found to have uncertainties of 0.763931611, 0.771259052, 0.772426358, 0.773017774, and 0.773910764. These uncertainties are all relatively high, with the uncertainty for the Method 1 calculation when at RPM 100 being the lowest. These high uncertainties may be a result of the many simplifications made during the experiment or uncertainty calculations. For instance, the pressure reading used to calculate the density was assumed to have no uncertainty. Furthermore, discrepancies could exist due to the distance between the Pitot-static probe that measured freestream velocity and the circular cylinder test section, potentially causing a difference in the experienced freestream velocity by the model. Also of note, the discrepancies are all of the same magnitude potentially alluding to a miscalculation or procedural error over a true inaccuracy in the calculations. This is further exemplified by the measurements made matching those by Bertin and Smith to a high degree. Regardless, the investigation overall met most of the objectives during the experimentation in the laboratory, albeit somewhat partially for objective three, and mostly succeeded in invalidating the inviscid theory for use in predicting pressure distributions, Reynolds number effects on pressure distributions, and wakes downstream.

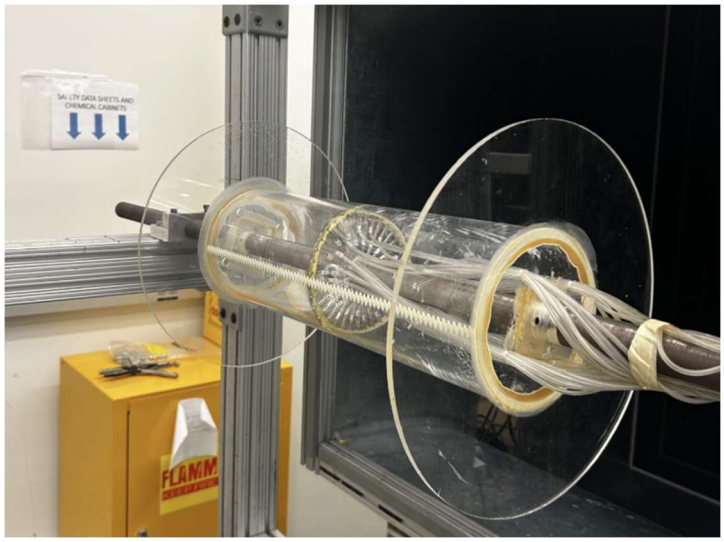

Fig. 1. Circular Cylinder Test Section.

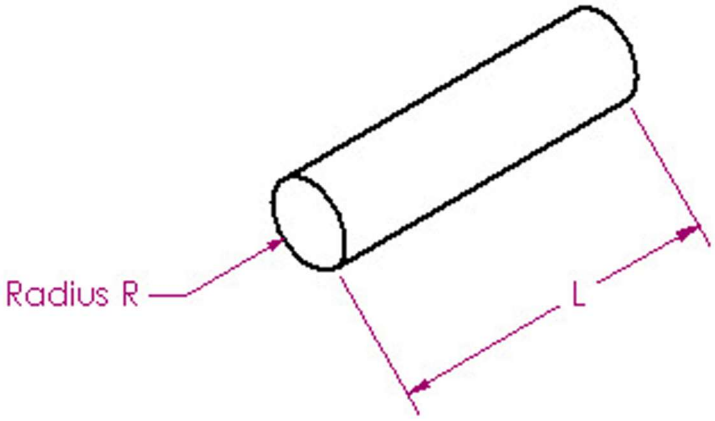

Fig. 2. Dimensions of the Cylinder from SolidWorks Drawing (Not to Scale).

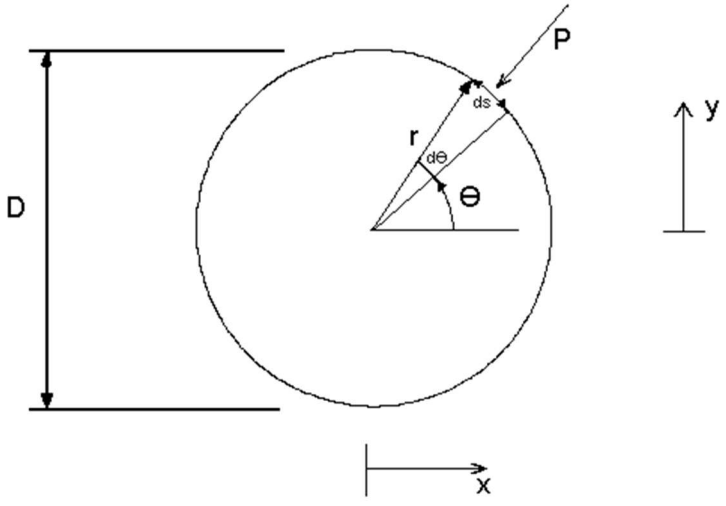

Fig. 3. Orientation of Cylinder Test Section and Theta Coordinate System.

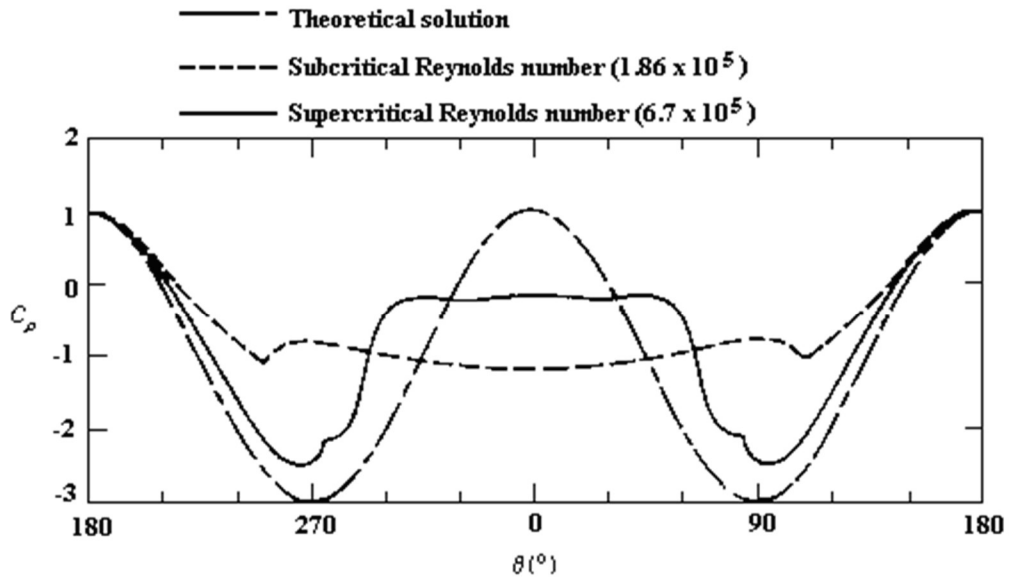

Fig. 4. Measured pressure distributions on a circular cylinder compared with a theoretical distribution calculated assuming ideal flow. From Bertin and Smith (1989), sourced from Borgoltz et. al (2006).

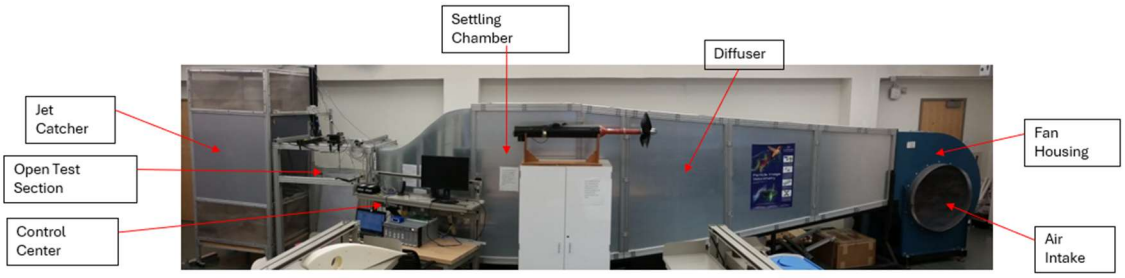

Fig. 5. Wind Tunnel Annotated.

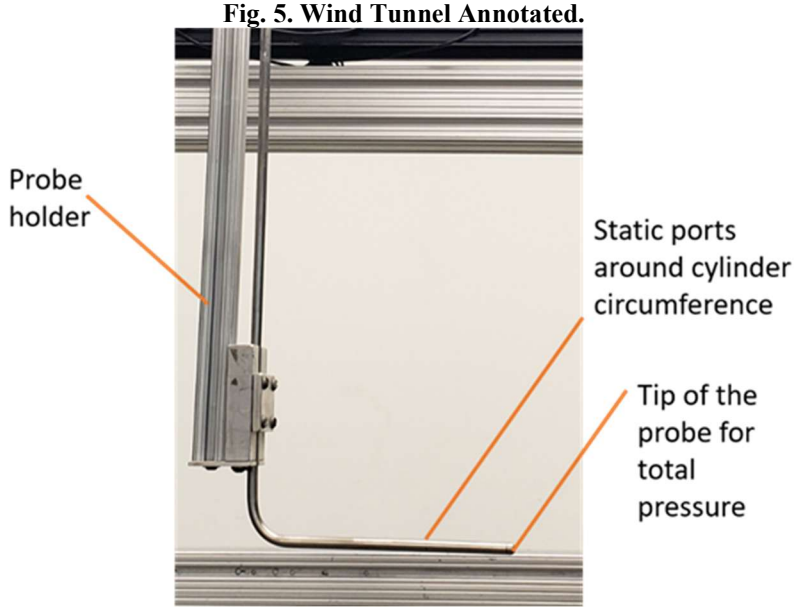

Fig. 6. Pitot-static probe annotated. From Borgoltz et. al (2006).

```
% EXP 3 plotting code
%02/20/25
clc;clear;close;
%% Params
theta = -180:10.285:180;
data = importdata('Obj1.txt');
pressure = data(1:36, 2);
pressure1 = data(1:36, 2)*248.8; %converting H20 to pa
diffp = ((946.77*100) - pressure1);
rho = 1.119; %kg/m^3
v = 2.247; %m/s
cpdata = pressure1./(0.5*rho*(v^2));
%% Plots
figure()
plot(theta, cpdata)
title('cp vs theta of the cylinder')
xlabel('theta (deg)')
ylabel('cp data')
ylim([-3 2])
grid on
```

Fig. 7. Code used for Fig 8.

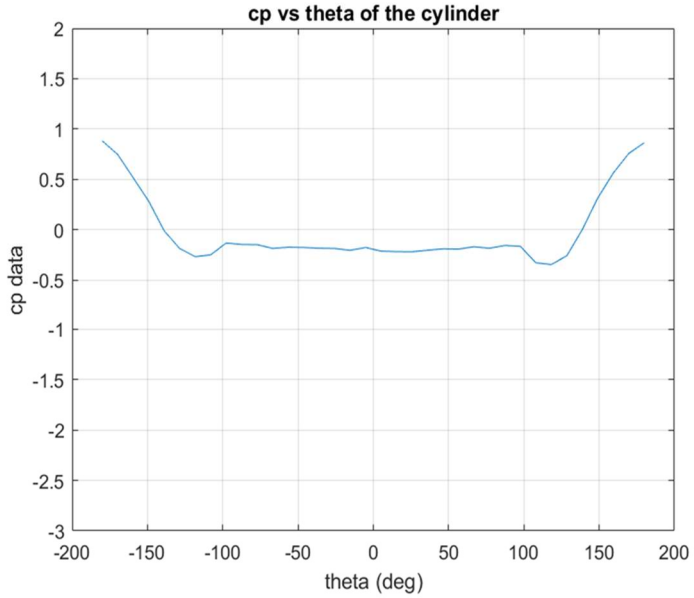

Fig. 8. Result of code for plotting pressure distribution on a circular cylinder.

```
theta = -180:10:180;
theta_rad = deg2rad(theta);
cp_theory = 1 - 4 * (sin(theta_rad)).^2;

% Plot Cp vs Theta
figure;
plot(theta, cp_theory);
xlabel('theta (deg)');
ylabel('cp predictions for theory');
title('cp vs theta of cylinder for theory');
grid on;
xlim([-180 180]);
ylim([-3 2]);
```

Fig. 9. Code used for Fig. 10.

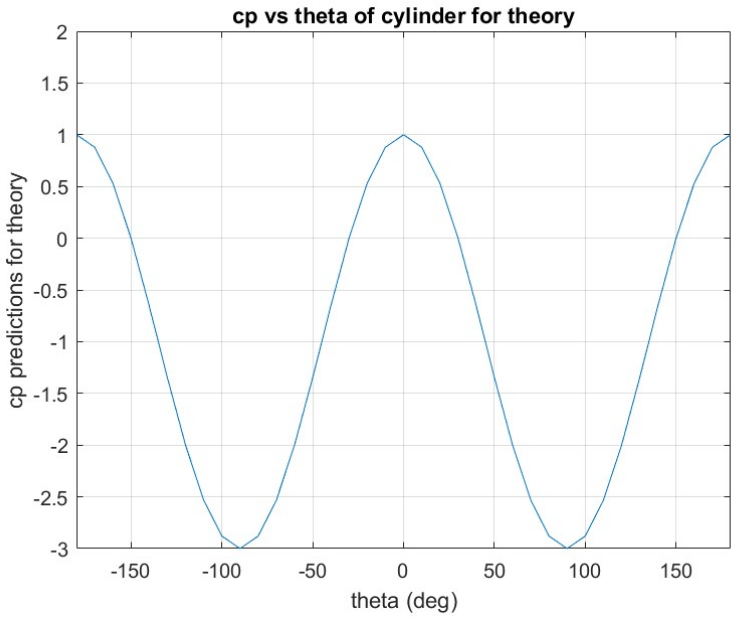

Fig. 10. Result of code used for inviscid theory pressure distribution on a circular cylinder.

```
% EXP 3 plotting code
%02/20/25
clc;clear;close;
%% Params
theta = -180:10.285:180;
data0 = importdata('Obj1.txt');
data1 = importdata('obj2_1.txt');
data2 = importdata('obj2_2.txt');
data3 = importdata('obj2_3.txt');
data4 = importdata('obj2_4.txt');

pressure0 = data0(1:36, 2)*248.8;
pressure1 = data1(1:36, 2)*248.8; %converting H20 to pa
pressure2 = data2(1:36, 2)*248.8; %converting H20 to pa
pressure3 = data3(1:36, 2)*248.8; %converting H20 to pa
pressure4 = data4(1:36, 2)*248.8; %converting H20 to pa
diffp0 = ((946.77*100) - pressure0);
diffp1 = ((946.77*100) - pressure1);
diffp2 = ((946.77*100) - pressure2);
diffp3 = ((946.77*100) - pressure3);
diffp4 = ((946.77*100) - pressure4);
rho = 1.119; %kg/m^3
v0 = 2.247;
v1 = 4.611047; %m/s
v2 = 7.010319;
v3 = 9.283959;
v4 = 11.648854;
cpdata0 = pressure0./(0.5*rho*(v0^2));
cpdata1 = pressure1./(0.5*rho*(v1^2));
cpdata2 = pressure2./(0.5*rho*(v2^2));
cpdata3 = pressure3./(0.5*rho*(v3^2));
cpdata4 = pressure4./(0.5*rho*(v4^2));
```

Fig. 11. Code used for Fig 12.

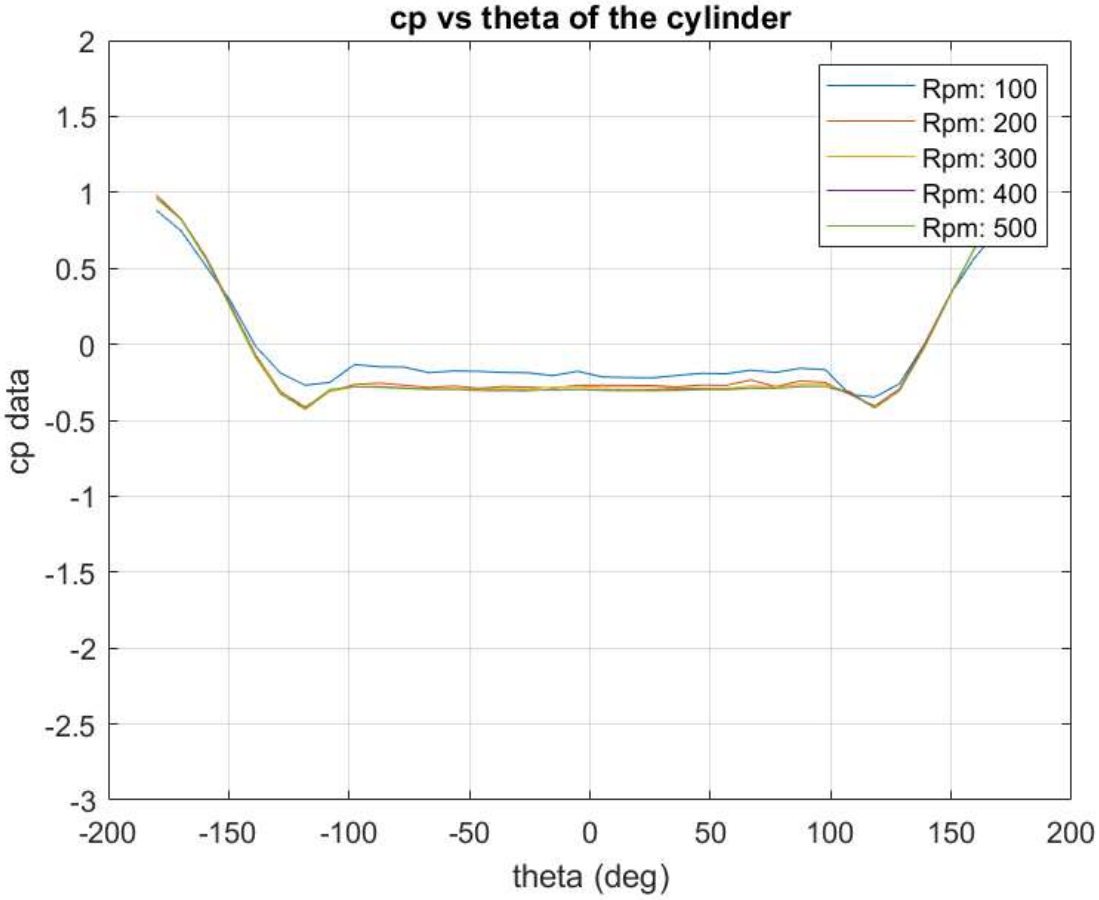

Fig. 12. Result of code used to plot multiple pressure distribution on a circular cylinder.

```
function idealFlowAirfoil()

    radius = 0.5;
    numPoints = 61;

    % Hardcoded circle coordinates
    theta = linspace(0, 2*pi, numPoints);
    x = radius * cos(theta) + 0.5;
    y = radius * sin(theta);

    alpha = 0; % Angle of attack in degrees

    [xc, yc, cp, cl, cmc4, gamma] = linearVortexPanelMethod(x, y, alpha);

    % Plot streamlines
    plotStreamlines(x, y, alpha, gamma);


end

function [xc,yc,cp,cl,cmc4,gamma]=linearVortexPanelMethod(x,y,alpha)
    z=x+i*y;alpha=alpha*pi/180                          %Coordinates as complex numbers, alpha in radians
    if(z(end)==z(1)) z=z(1:end-1);end                   %Delete repeated end point, if needed
    npanels=length(z);k=npanels;                        %No. of panels, Kutta condition
    a=[1:npanels];b=[2:npanels 1];c=[3:npanels 1 2];    %Panel indices
    dzds=(z(b)-z(a))./abs(z(b)-z(a));                   %Panel slopes
    eps=0.0001;zc=(z(a)+z(b))/2-i*eps*(z(b)-z(a));      %Control points
    winf=exp(-i*alpha);                                 %Free stream velocity

    cm=zeros(npanels);                                  %Calculate influence coefficients and result vector
    for m=1:npanels
    cm(:,m)=-i*(((zc(m)-z(a))./(z(b)-z(a)).*log((zc(m)-z(a))./(zc(m)-z(b)))-1)./dzds(a)/2/pi...
              -((zc(m)-z(c))./(z(b)-z(c)).*log((zc(m)-z(c))./(zc(m)-z(b)))-1)./dzds(b)/2/pi)*dzds(m);
    end
    cm1=imag(cm);cm1(:,end)=0;cm1(k,end)=1;
    res=imag(-winf*dzds);res(end)=0;

    gamma=res/cm1;                                          %Solve for panel strengths

    ut=real(gamma*cm+winf*dzds);cp=1-ut.^2/abs(winf).^2;    %Calculate Cp distribution
    cn=sum(cp.*real(z(b)-z(a)));ca=-sum(cp.*imag(z(b)-z(a)));
    cl=cn*cos(alpha)-ca*sin(alpha);                         %Calculate Cl, Cm about quarter chord
    cmc4=sum(cp.*real(z(b)-z(a)).*(0.25-real(zc))-cp.*imag(z(b)-z(a)).*imag(zc));
    xc=real(zc);yc=imag(zc);                                %Evaluate control point coordinates
end

function plotStreamlines(x,y,alpha,gamma)
    figure;ps=get(gcf,'Position');set(gcf,'Position',[ps(1)+77 ps(2)-83 ps(3) ps(4)]);
    z=x+i*y;alpha=alpha*pi/180                          %Coordinates as complex numbers, alpha in radians
    if(z(end)==z(1)) z=z(1:end-1);end                   %Delete repeated end point, if needed
    npanels=length(z);                                  %No. of panels
    a=[1:npanels];b=[2:npanels 1];c=[3:npanels 1 2];    %Panel indices
    dzds=(z(b)-z(a))./abs(z(b)-z(a));                   %Panel slopes
    eps=0.0001;zc=(z(a)+z(b))/2-i*eps*(z(b)-z(a));      %Control points
    winf=exp(-i*alpha);                                 %Free stream velocity
    plot([z(a);z(b)],'k');hold on;plot(zc,'k.');axis image;
    title('Click on plot to start streamline, outside plot to exit');
    xl=-0.5;xh=1.5;yl=-1;yh=1;axis([xl xh yl yh]);
    streamstep=.01;
    [x,y]=ginput(1);
    while x>xl & x<xh & y>yl & y<yh
        cntr=0;
        while x>xl & x<xh & y>yl & y<yh & cntr<5000
            zp=x+i*y;
            w=winf-gamma*i*(((zp-z(a))./(z(b)-z(a)).*log((zp-z(a))./(zp-z(b)))-1)./dzds(a)/2/pi...
               -((zp-z(c))./(z(b)-z(c)).*log((zp-z(c))./(zp-z(b)))-1)./dzds(b)/2/pi).';
            x1=x+streamstep*real(w)/abs(w);y1=y-streamstep*imag(w)/abs(w);zp=x1+i*y1;
            w1=winf-gamma*i*(((zp-z(a))./(z(b)-z(a)).*log((zp-z(a))./(zp-z(b)))-1)./dzds(a)/2/pi...
               -((zp-z(c))./(z(b)-z(c)).*log((zp-z(c))./(zp-z(b)))-1)./dzds(b)/2/pi).';
            w=(w+w1)/2;
            x1=x+streamstep*real(w)/abs(w);y1=y-streamstep*imag(w)/abs(w);
            plot([x x1],[y y1],'b-');
            x=x1;y=y1;cntr=cntr+1;
        end
        [x,y]=ginput(1);
    end
    hold off;title('');
```

Fig. 13. Code Used to Generate Fig. 14.

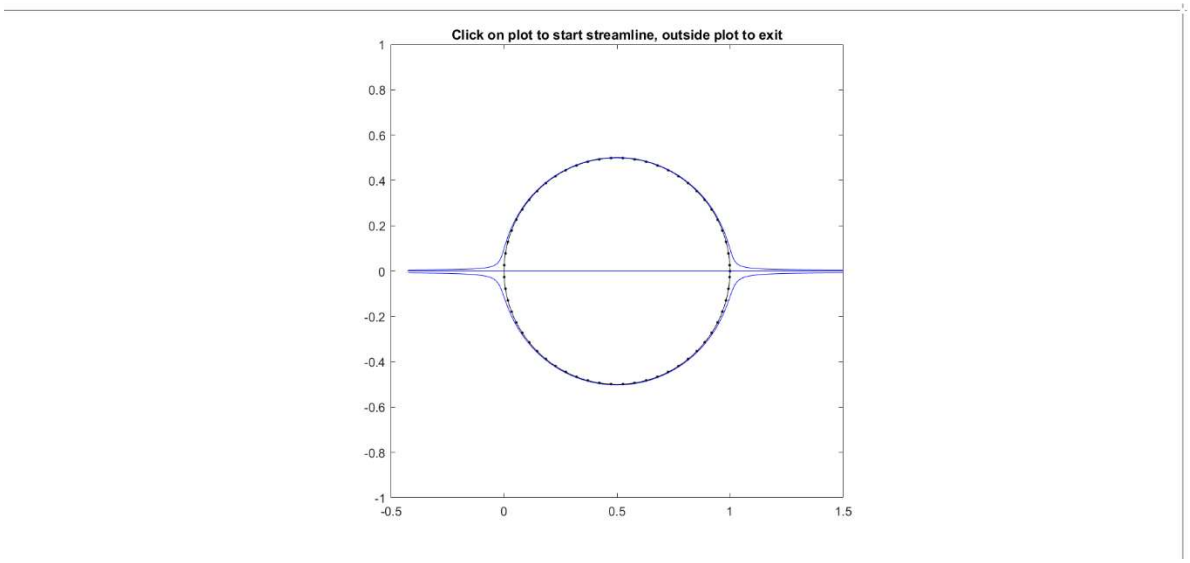

Fig. 14. Result of code used to plot streamlines above, at, and under the centerline of a circle according to inviscid theory.

REFERENCES

Borgoltz, A., Deveneport, W. J., and Intaratep, N., 2006, AOE 3054 Experimental Methods Course Manual. Experiment 3 - Flow Over a Circular Cylinder, A.O.E. Department, Virginia Tech. Blacksburg VA.

Bertin, J. J., 2009, Aerodynamics for Engineers, 5th ed., Pearson Prentice Hall, Upper Saddle River, NJ, Fig. 3.17, p. 123.

Appendix

A. Uncertainty Analysis

In order to perform uncertainty analysis, the primary uncertainties, which involve physical errors in calculations due to equipment limitations, are calculated and combined to get a total uncertainty using the equation

$$\delta(R) = \sqrt{\frac{\partial R}{\partial a}^2 \delta(a)^2 + \frac{\partial R}{\partial b}^2 \delta(b)^2 + \cdots} \quad (10)$$

Shown in Table 10, 11, 12, 13, and 14 below are the calculation of uncertainties for the coefficient of pressure calculations performed in Method 1 and Method 2 for the various RPMs. Uncertainties arise from the tolerances of instrumentation such as the thermometer and the Pitot-static probe's ability to measure freestream velocity. Assumptions are inherently made through the calculation of the air density which relies on the instrumentation used to measure ambient pressure having no uncertainty. As a result of these primary uncertainties, further derived uncertainties from the tabulation of the air density and differential pressure are also calculated and shown.

Table 10. Table for calculation of uncertainty in the coefficient of pressure for 100 RPM.

Variables	*Quantity*	*Primary Uncertainty*	*a+da, b, c, d*	*a, b+db, c, d*	*a, b, c+dc, d*	*a,b,c,d+dd*
Velocity	2.084728	0.1	2.084728	2.184728	2.084728	2.084728
Thermometer	21.687	0.5	21.687	21.687	22.187	21.687
Intermediate Results						
Differential Pressure mbar	0.009496	0.1	0.009496	0.009496	0.009496	0.009496
Air Density, kg/m^3	1.11935		1.11935	1.11935	1.11935	1.11935
Final Results						
C_p	0.390396575		0.39039657	0.35547580	0.39039657	0.39039657
Uncertainty of C_p	0.763931611					

From the tabulations in Table 10, the uncertainty is found to be 0.763931611.

Table 11. Table for calculation of uncertainty in the coefficient of pressure for 200 RPM.

Variables	*Quantity*	*Primary Uncertainty*	*a+da, b, c, d*	*a, b+db, c, d*	*a, b, c+dc, d*	*a,b,c,d+dd*
Velocity	4.611047	0.1	4.611047	4.711047	4.611047	4.611047
Thermometer (Deg C)	20.875	0.5	20.875	20.875	21.375	20.875
Intermediate Results						
Differential Pressure mbar	0.046403	0.1	0.046403	0.046403	0.046403	0.046403
Air Density, kg/m^3	1.122691		1.11935	1.11935	1.11935	1.11935
Final Results						
C_p	0.388792		0.388791568	0.373572825	0.389951911	0.389951911

Uncertainty of C_p	0.771259052	

From the tabulations in Table 11, the uncertainty is found to be 0.771259052.

Table 12. Table for calculation of uncertainty in the coefficient of pressure for 300 RPM.

Variables	*Quantity*	*Primary Uncertainty*	*a+da, b, c, d*	*a, b+db, c, d*	*a, b, c+dc, d*	*a,b,c,d+dd*
Velocity	7.0103	0.1	7.0103	7.1103	7.0103	7.0103
Thermometer (Deg C)	21.75	0.5	21.75	21.75	22.25	21.75
Intermediate Results						
Differential Pressure mbar	0.106972	0.1	0.106972	0.106972	0.106972	0.106972
Air Density, kg/m^3	1.119583677		1.11935	1.11935	1.11935	1.11935
Final Results						
C_p	0.388839		0.388839473	0.378057935	0.388920648	0.388920648
Uncertainty of C_p	0.772426358					

From the tabulations in Table 12, the uncertainty is found to be 0.772426358.

Table 13. Table for calculation of uncertainty in the coefficient of pressure for 400 RPM.

Variables	*Quantity*	*Primary Uncertainty*	*a+da, b, c, d*	*a, b+db, c, d*	*a, b, c+dc, d*	*a,b,c,d+dd*
Velocity	9.2839	0.1	9.2839	9.3839	9.2839	9.2839
Thermometer (Deg C)	21.875	0.5	21.875	21.875	22.375	21.875
Intermediate Results						
Differential Pressure mbar	0.187422	0.1	0.187422	0.187422	0.187422	0.187422
Air Density, kg/m^3	1.119094319		1.11935	1.11935	1.11935	1.11935
Final Results						
C_p	0.388618		0.388618047	0.380292638	0.388529279	0.388529279
Uncertainty of C_p	0.773017774					

From the tabulations in Table 13, the uncertainty is found to be 0.773017774.

Table 14. Table for calculation of uncertainty in the coefficient of pressure for 500 RPM.

Variables	*Quantity*	*Primary Uncertainty*	*a+da, b, c, d*	*a, b+db, c, d*	*a, b, c+dc, d*	*a,b,c,d+dd*
Velocity	11.6488	0.1	11.6488	11.7488	11.6488	11.6488
Thermometer (Deg C)	22	0.5	22	22	22.5	22
Intermediate Results						
Differential Pressure mbar	0.295057	0.1	0.295057	0.295057	0.295057	0.295057
Air Density, kg/m^3	1.118474218		1.11935	1.11935	1.11935	1.11935
Final Results						
C_p	0.388819075		0.388819075	0.381929314	0.388514862	0.388514862
Uncertainty of C_p	0.773910764					

From the tabulations in Table 14, the uncertainty is found to be 0.773910764.